Electronic Journal of Biotechnology 74 (2025) 19–28

Contents lists available at ScienceDirect

Electronic Journal of Biotechnology

journal homepage: www.elsevier.com/locate/ejbt

Research article

Green synthesis of silver nanoparticles using *Viola odorata* and *Onosma hispidum*: Evaluation of their antimicrobial, antioxidant, and hemolytic properties against multidrug-resistant microbes ☆,☆☆

Aneeta Andleeb [a,1], Aneeza Khalid [a,1], Sadia Khalil [a], Hammad Arshad [a,b], Saima Sadaf [a,*]

[a] School of Biochemistry and Biotechnology, University of the Punjab, Quaid-e-Azam Campus, Lahore, Pakistan
[b] Department of Biology, Lahore Garrison University, Lahore, Pakistan

GRAPHICAL ABSTRACT

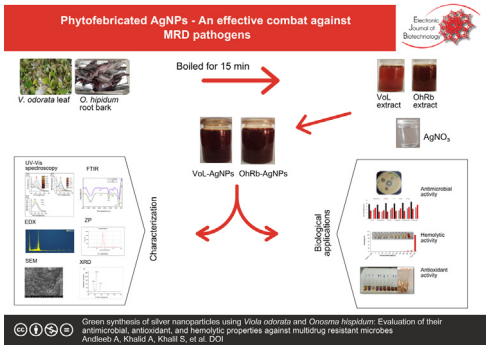

ARTICLE INFO

Article history:
Received 24 February 2024
Accepted 2 December 2024
Available online 05 February 2025

Keywords:
Antimicrobial
Antimicrobial resistance
Antioxidant
Green synthesis
Hemolysis assay
Hemolytic properties
Multidrug resistant bacteria
Nanoparticles
Onosma hispidum
Silver nanoparticles
Viola odorata

ABSTRACT

Background: Rapid increase in antimicrobial resistance poses a significant threat to global health, necessitating alternative strategies to combat multi-drug resistant (MDR) pathogens. Advances in nanobiotechnology may offer promising solutions to this pressing issue. This study revolves around developing an efficient method for synthesizing silver nanoparticles (AgNPs) based on aqueous extracts of *Viola odorata* leaves (VoL) and *Onosma hispidum* root barks (OhRb), traditional medicinal perennial herbs, followed by evaluating their antioxidant and antimicrobial potential against MDR pathogens.
Results: The synthesis of nanoparticles was completed in 15–20 min at 55–60°C using green approach. The characterized AgNPs showed significant antimicrobial activity against *Escherichia coli, Pseudomonas aeruginosa, Klebsiella pneumoniae*, *Staphylococcus aureus, Streptococcus agalactiae*, and *Candida albicans*, with zones of inhibition ranging from 12 mm ± 0.636 to 25 mm ± 0.282. Minimum inhibitory concentration and minimum bactericidal concentrations ranged from 0.39 to 6.125 µg/mL. Additionally, the nanoparticles demonstrated significant antioxidant potential compared to the aqueous plant extracts. Importantly, the investigation into the effects of the nanoparticles on red blood cells revealed no pronounced hemolysis even at higher concentrations (300 µg/mL) of VoL-AgNPs and OhRb-AgNPs, demonstrating their biocompatibility and hemolytic safety profile.
Conclusions: The VoL-AgNPs and OhRb-AgNPs exhibit appreciable antimicrobial and antioxidant activities with minimal hemolysis, underscoring their potential to combat MDR pathogens, and further

☆ Audio abstract available in Supplementary material.
Peer review under responsibility of Pontificia Universidad Católica de Valparaíso
* Corresponding author.
E-mail address: saima.sbb@pu.edu.pk (S. Sadaf).
[1] These authors contributed equally to this work.

https://doi.org/10.1016/j.ejbt.2024.12.003

applicability in therapeutic settings. However, *in vivo* studies are warranted to explore their biomedical applications, such as in wound dressings and treatments for disorders caused by free radical damage.
How to cite: Andleeb A, Khalid A, Khalil S, et al. Green synthesis of silver nanoparticles using *Viola odorata* and *Onosma hispidum*: Evaluation of their antimicrobial, antioxidant, and hemolytic properties against multidrug resistant microbes. Electron J Biotechnol 2025;74. https://doi.org/10.1016/j.ejbt.2024.12.003.

1. Introduction

The frequent and unnecessary use of antibiotics, in addition to natural evolutionary processes, has paved the way for microbes to develop resistance against a wide range of antibiotics, which not only leads to prolonged illnesses but also impacts both the quality and expectancy of life. Projections indicate that in the absence of serious and significant global efforts to control and address the antimicrobial resistance, the annual death toll may escalate from 0.7 million to a staggering 10 million by the year 2050 [1,2]. Since developing new antibiotics is a challenging process requiring several years of efforts to ensure safety, stability, and efficacy as well as navigating complex regulatory pathways for market approval, there exists a pressing need to explore alternative strategies to tackle multi-drug resistant (MDR) pathogens [3,4].

Over the past decade, the myriad applications of nanotechnology and nanoparticles (NPs) have catalyzed notable advancements in nearly every facet of biological science and technology. Contrasting their 'macroparticle' counterparts, the NPs have a variety of advantages including better action due to a greater surface area, unique physiochemical characteristics, and requirement for less material [4,5]. Among the metal-based NPs, silver (Ag) NPs constitute a significant class of nanomaterials with applications in fields as diverse as optics, electronics, food industry, catalysis, physics, healthcare, medicine, ecological remediation, and development of nanodevices [4,6]. Further, it has been observed that the antimicrobial properties of existing antibiotics can be enhanced in synergy with AgNPs thus reducing the dosage of antibiotics and duration of use while hampering the AMR development, in parallel [5,6,7].

Whereas physical and chemical methods for the synthesis of AgNPs are well-established, their broader applicability and effectiveness are hindered by limitations such as: the use of hazardous substances, generation of toxic by-products, high energy consumption, low yield, and a broad size range of synthesized particles [4,5,8]. Hence, there is a preference for environmentally benign approaches, utilizing ingredients like microbial biomass, natural chemicals, and plant extracts. In particular, the use of plant extracts in the production of NPs is favored over microbial-based systems due to their simplicity, safety, and convenience, eliminating the need for maintaining complex cell cultures [8,9].

The chemical substances, which are mostly found in plant extract, include proteins, alkaloids, flavonoids, terpenoids, and reducing sugars that reduce Ag^+ to generate AgNPs [7,10]. These bioactive compounds not only provide antioxidant effects but also contribute directly to therapeutic activities. In therapies like anticancer treatments, antioxidant NPs can protect healthy cells from oxidative damage caused by chemotherapy or radiation, thereby reducing side effects and improving patient outcomes. By neutralizing reactive oxygen species (ROS), the antioxidant NPs prevent cellular damage - a common underlying factor in various pathological conditions and ailments [4,7,8,10].

Several studies have explored the synthesis and biomedical applications of NPs employing extracts from various plants like *Phoenix dactylifera* [11], *Allium sativum* [12], *Allium eriophyllum* [13], *Tamarindus indica* [14], *Thymus fedtschenkoi* [15], *Achillea biebersteinii* [16], *Rumex nervosus* [17], *Citrus limon* [18], *Acacia cyanophylla* [19], *Ferula persica* [20], and others [21]. We in the present study have used two perennial herbs i.e.:

(1) *Viola odorata* (commonly known as Gul-e-Banafsha, sweet violet, or English violet), which is a key ingredient in 'Joshanda'- a herbal remedy known for its effectiveness against the flu, colds, and cough.
(2) *Onosma hispidum*, which is commonly known as Ratanjot and is documented for its red dye-producing roots.

V. odorata exhibits substantial anticancer, antimicrobial, anti-inflammatory, and cytotoxic activities [22,23]. Likewise, *O. hispidum* roots are widely used in oils, pharmaceutical preparations, and foods and are effective in treating wounds, fever, cancer, diabetes, infectious diseases, and pain [24,25].

To the best of our knowledge, the synthesis of silver nanoparticles utilizing the aqueous extract of *V. odorata* leaves (VoL) and *O. hispidum* root bark (OhRb) has not yet been investigated. Given the immense medicinal significance of these plants, this research aims to develop a simple, rapid, and sustainable method for the biosynthesis of VoL- and OhRb-based nanoparticles, with the goal of enhancing their antimicrobial, antioxidant, and hemolytic properties for improved biomedical applications. The findings have the potential to offer valuable insights into alternative strategies for combating MDR pathogens and addressing the growing challenges of antibiotic resistance.

2. Materials and methods

2.1. Synthesis of VoL-AgNPs and OhRb-AgNPs

Fresh VoL was collected from Azad Jammu and Kashmir, while dried OhRb were sourced from a nursery in Lahore. Both plant materials were thoroughly washed with tap- and distilled water to remove contaminants, dried and then sliced into small pieces. To prepare 10% extract (w/v), 10 g of each plant part was boiled in 100 mL distilled water for 15 min. The extracts were cooled, filter sterilized and stored at 4°C [26]. For the synthesis of nanoparticles, the VoL and OhRb extracts were separately mixed with 10 mM $AgNO_3$ solution at varying ratios of 9:1, 8:2, 7:3, 6:4 and 5:5. AgNPs formation was tested at $AgNO_3$ concentrations ranging from 1 to 30 mM, with the reaction temperatures ranging between 50–60°C to determine the optimal temperature conditions. After identifying the best extract-to-$AgNO_3$ ratios and concentrations, pH studies (pH 7–10) were conducted to understand its impact on the synthesis of NPs [27]. Finally, the synthesized AgNPs were purified by centrifuging at 4500 rpm and 25°C for 15 min.

2.2. Characterization of VoL-AgNPs and OhRb-AgNPs

The synthesis of VoL-AgNPs and OhRb-AgNPs was followed by observing the color change in the solutions. Additionally, their absorbance was measured using a UV–Vis spectrophotometer (Model: C-7200, PEAK Instrument, USA) over a wavelength range of 300–800 nm. To analyze the functional groups, present in both

the plant extracts and the nanoparticles, FTIR spectral analysis was conducted using a spectrometer (IR Prestige-21, Shimadzu, Japan) with KBr pellets, covering the spectral range of 4000–400 cm^{-1}. The morphology and elemental composition of the synthesized VoL-AgNPs and OhRb-AgNPs were examined through scanning electron microscopy (SEM) and energy dispersive X-ray (EDX) analysis (FEI Nova 450 NanoSEM). The crystalline structure of the nanoparticles was further analyzed using X-ray diffraction (XRD; MiniFlex600-C). The Zetasizer nano series (Malvern Zetasizer Nano ZSP) was employed to measure the zeta potential (ZP) and determine the size of VoL-AgNPs and OhRb-AgNPs.

2.3. Antimicrobial activity

The antimicrobial activity of VoL-AgNPs and OhRb-AgNPs was assessed using the Kirby-Bauer method [28] against gram-negative bacteria (*E. coli*, *P. aeruginosa*, and *K. pneumoniae*), gram-positive bacteria (*S. aureus* and *S. agalactiae*), and fungal strain *C. albicans*. Sterile Mueller Hinton Agar (MHA) was added to Petri plates and allowed to solidify under aseptic conditions. Bacterial cultures prepared according to McFarland's standard protocol were transferred onto the MHA plates. Discs containing 50 and 75 µg of synthesized VoL-AgNPs and OhRb-AgNPs were placed on the plates. For comparison, 10 µL of antibiotic amikacin (30 µg), $AgNO_3$ (10 mM), and VoL/OhRb extracts were also applied. After 24 h of incubation at 37°C, the zones of inhibition (ZOI) were measured. The minimum inhibitory concentration (MIC) and minimum bactericidal concentration (MBC) of VoL-AgNPs and OhRb-AgNPs were also determined using the two-fold serial macro-dilution method. Briefly, serial dilutions of the AgNPs were prepared in test tubes, with concentrations ranging between 0.195 and 50 µg/mL. The bacterial inoculum was standardized to 10^8 CFU/mL (0.5 McFarland standard). 10 mM $AgNO_3$ was used as the positive control, and inoculum alone served as the negative control. The test tubes were incubated overnight at 37°C. After incubation, the MIC was determined as the lowest concentration of the nanoparticles that visibly inhibited bacterial growth. The MBC was assessed by subculturing the suspensions from test tubes that showed no bacterial growth onto fresh MHA plates at concentrations equal to or higher than the MIC. For MBC determination, 10 µL of the suspension from test tubes with no visible bacterial growth was spread onto MHA plates and incubated at 37°C for 24 h. The MBC was identified by visually confirming the absence of bacterial colonies on the plates.

2.4. Antioxidant activity

With slight modifications to the methodology by Sreelekha et al. [29], the antioxidant activity of VoL-AgNPs and OhRb-AgNPs was evaluated using the 2,2-diphenyl-1-picrylhydrazyl (DPPH) free radical scavenging assay. Ascorbic acid was used as the positive control, and ethanol as the negative control. To perform the assay, 2 mL of freshly prepared DPPH solution (0.1 mM in ethanol) was mixed with 1 mL of different concentrations of VoL-AgNPs or OhRb-AgNPs (50, 75, and 100 µg/mL). The mixtures were thoroughly shaken and then incubated in the dark for 30 min. After incubation, the absorbance of each sample was measured using a UV–Vis spectrophotometer at a wavelength of 517 nm. The percentage inhibition of DPPH was then calculated to assess the antioxidant potential of NPs as described earlier [29].

2.5. Hemolytic activity assessment

For *in vitro* hemolytic activity assessment of VoL-AgNPs and OhRb-AgNPs, fresh human blood was collected in EDTA tubes

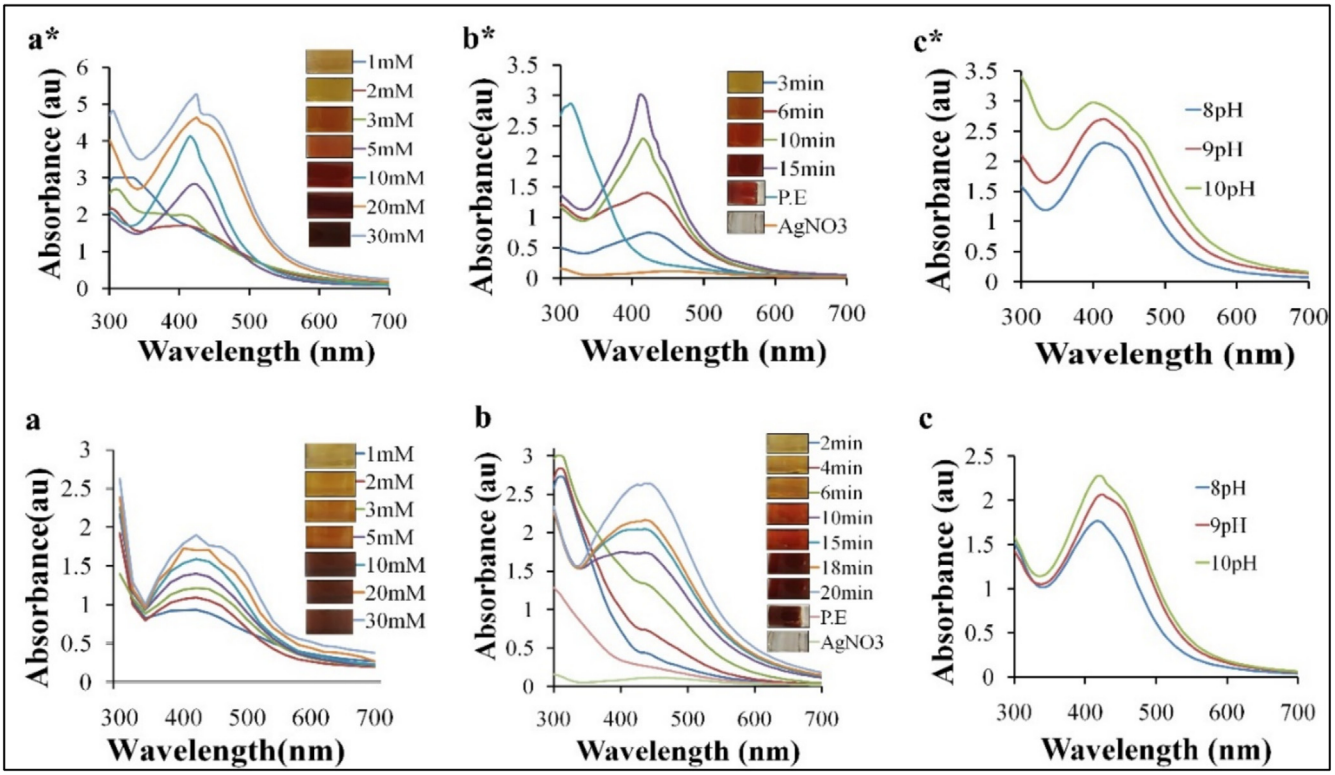

Fig. 1. UV–vis spectrum of VoL-AgNPs (a*, b*, c*) and OhRb-AgNPs (a, b, c). The **a*** and **a** depict various concentrations of $AgNO_3$ used (1, 2, 3, 5, 10, 20, and 30 mM), while **b*** and **b** represent a thorough time-based synthesis for VoL-AgNPs and OhRb-AgNPs. The **c*** and **c** show the impact of different pH values on the production of VoL-AgNPs and OhRb-AgNPs. Every sample shows absorbance maxima between 400 and 440 nm.

and washed with phosphate-buffered saline (PBS) at 4,000 rpm for 5 min. The red blood cells (RBCs) were rinsed with PBS and washed twice to ensure the removal of residual contaminants. For assay, 800 µL of each AgNPs sample was added to sterile tubes containing 200 µL of diluted RBCs, resulting in final concentrations of 5, 10, 20, 30, 40, 50, 100, 150, 200, 250, and 300 µg/mL. Triton X-100 (displaying hemolytic effect) and saline solution were used as positive and negative controls, respectively. The tubes were incubated at 37°C for 1 h, followed by centrifugation. The supernatants were collected, and the optical density (OD) was measured at 570 nm. The percentage of hemolysis was calculated using the formula outlined by Parthiban et al. [30].

3. Results

3.1. Synthesis of eco-friendly nanoparticles

The VoL- and OhRb-based, ecofriendly nanoparticles were successfully synthesized in less than 20 min at temperatures 55°C and 60°C, respectively (Fig. 1).

Time-dependent analysis revealed that NP formation began within 10 min of incubation using plant extract with 10 mM $AgNO_3$ in a ratio of 9:1 for VoL and 8:2 for OhRb. The optimal synthesis, however, was observed at 15 min for VoL-AgNPs and 20 min for OhRb-AgNPs, as depicted in Fig. 1b*, Fig. 1b. The characteristic surface plasmon resonance (SPR) absorption bands were observed at 420 nm for VoL-AgNPs and 430 nm for OhRb-AgNPs.

The pH of reaction mixture also played a crucial role in NPs synthesis, as variations in pH caused shifts in absorption peaks. For both VoL-AgNPs and OhRb-AgNPs, these peaks ranged between 400 and 440 nm, as shown in Fig. 1c*, Fig. 1c.

3.2. Characterization of nanoparticles using SEM, EDX, FTIR analysis

The results of the SEM and EDX analyses for VoL-AgNPs and OhRb-AgNPs are presented in Fig. 2. The SEM images (Fig. 2A and Fig. 2B) demonstrate the presence of nano-sized, spherical AgNPs.

The EDX analysis provided more details on the elemental compositions of VoL-AgNPs and OhRb-AgNPs. Both spectra showed a strong peak for Ag acquired at 3 keV^{+}, confirming the successful reduction of $AgNO_3$ into AgNPs (Fig. 2A3 and Fig. 2B3). Additionally, faint signals for gold, oxygen, chlorine, and carbon were observed, suggesting the presence of phytoconstituents from the plant extracts on the surface of the AgNPs.

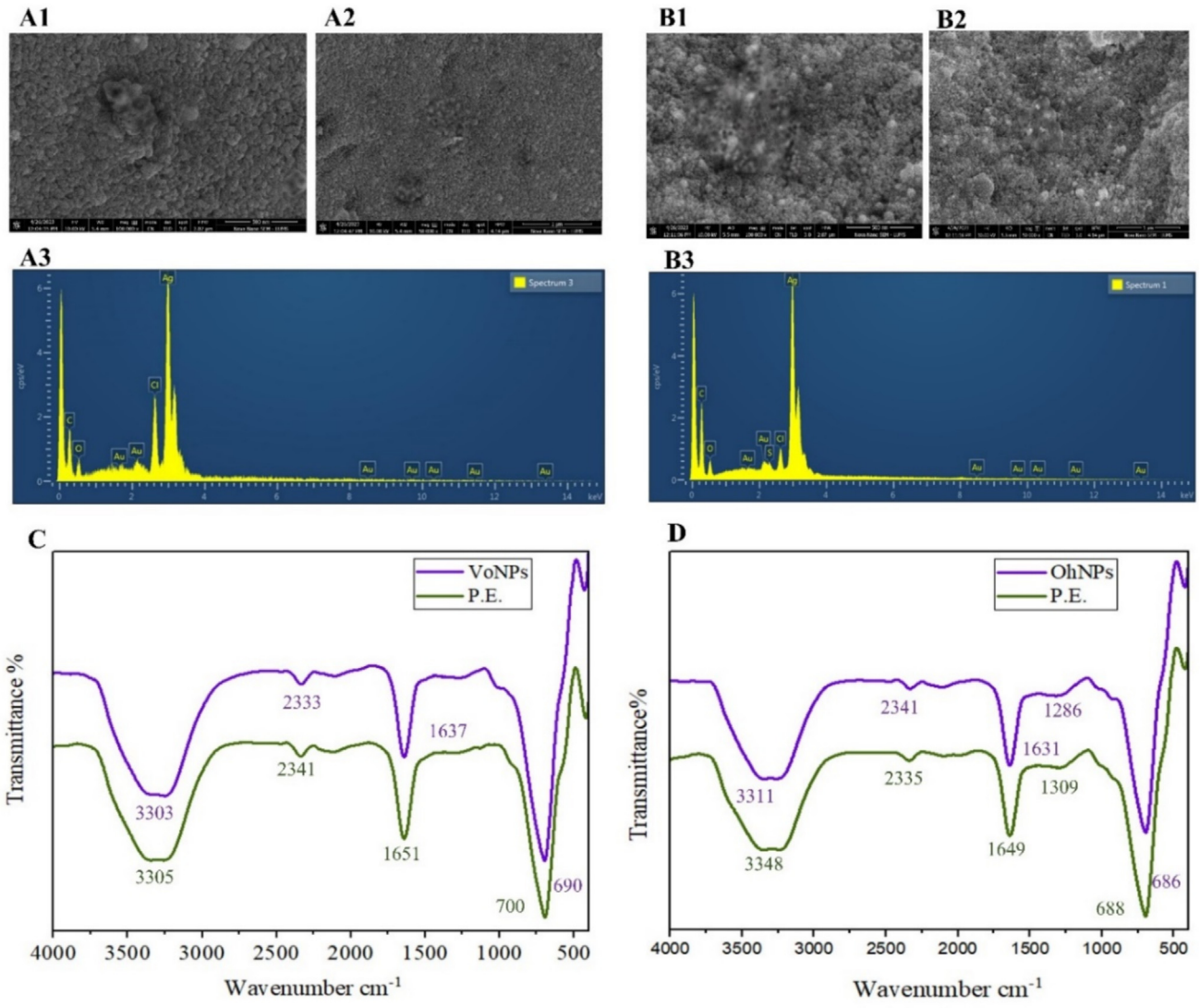

Fig. 2. The SEM, EDX, and FTIR analyses of VoL-AgNPs and OhRb-AgNPs. Panels A1 and A2 present SEM images of VoL-AgNPs, while B1 and B2 depict those of OhRb-AgNPs. Panels A3 and B3 show the EDX spectra of VoL-AgNPs and OhRb-AgNPs, respectively. Panels C and D illustrate the FTIR spectra of VoL and OhRb, confirming the presence of functional groups involved in the reduction process during AgNP synthesis.

The FTIR analysis showed that the plant extracts, VoL-AgNPs, and OhRb-AgNPs, exhibit almost identical infrared (IR) bands (Fig. 3C, Fig. 3D). For the VoL extract, absorbance peaks were observed at 3313.70, 2341.58, 1651.06, 1290.377, and 700.16 cm^{-1}, while for VoL-AgNPs at 3305.99, 2333.86, 1637.56, 1255.65, and 690.51 cm^{-1}. In the case of OhRb extract, the peaks were seen at 3349.42, 2335.79, 1649.37, 1309.66, and 680.58 cm^{-1}, whereas OhRb-AgNPs showed peaks at 3317.77, 2328.08, 1631.77, 1286.52, and 686.65 cm^{-1}. The peaks at a range of 3650–3200 cm^{-1}, 1630–1680 cm^{-1}, 1000–1320 cm^{-1}, and 730–550 cm^{-1} respectively correspond to O—H, C═O, C—O, and C—Cl stretching. Additional peaks at 2341, 2333, 2328, and 2335 cm^{-1} indicated weak C═N and C—H stretching, likely due to the presence of aromatic compounds and nitriles in the AgNPs while the peak at 2341 cm^{-1} is attributed to C—H stretching.

3.3. Analysis of X-ray diffraction pattern and zeta potential

The crystallinity of AgNPs was examined using XRD analysis, and the patterns for VoL-AgNPs and OhRb-AgNPs are illustrated in Fig. 3A and Fig. 3B. The distinct peaks for VoL-AgNPs appeared at angles of 27.86°, 32.15°, and 38.1°, corresponding to the crystallographic planes (210), (122), and (111). In contrast, OhRb-AgNPs exhibited peaks at 23.15°, 27.21°, 29.69°, 32.34°, 38.2°, and 43.65°, associated with planes (010), (210), (011), (122), (111), and (012), respectively. These peaks confirm the crystalline structures of both types of AgNPs, consistent with the standard AgNP XRD pattern from JCPDS file number 04-0783.

Further, the zeta potential analysis (Fig. 3C, Fig. 3E) showed prominent peaks for VoL-AgNPs at –25.7 mV and for OhRb-AgNPs at –23.5 mV, indicating that biomolecules may be capping

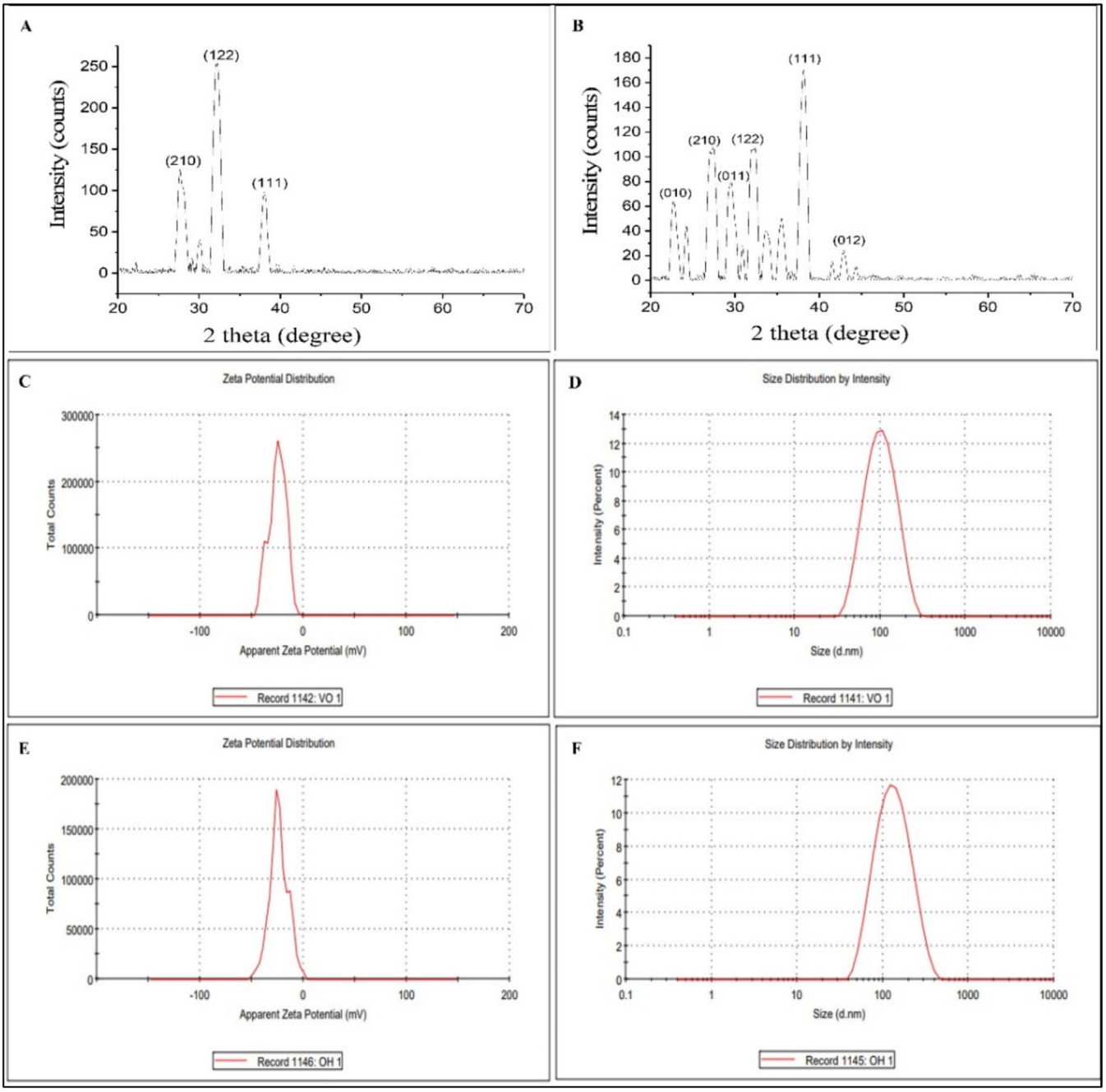

Fig. 3. XRD and ZP of the AgNPs produced from aqueous extracts of VoL and OhRb. A and B depicted the XRD pattern of VoL-AgNPs and OhRb-AgNPs, respectively, while C and E depicted the ZP and D and F depicted the size analysis results of VoL-AgNPs and OhRb-AgNPs, respectively.

the AgNPs. The single peaks suggest that both types of nanoparticles are stable. Average size distribution of VoL-AgNPs and OhRb-AgNPs was determined to be 79.92 ± 45.61 nm and 106 ± 68.01 n m, respectively (Fig. 3D, Fig. 3F).

3.4. Antimicrobial activity

The antimicrobial activity of VoL and OhRb extracts, 10 mM $AgNO_3$ solution, biosynthesized VoL-AgNPs, OhRb-AgNPs, and ami-

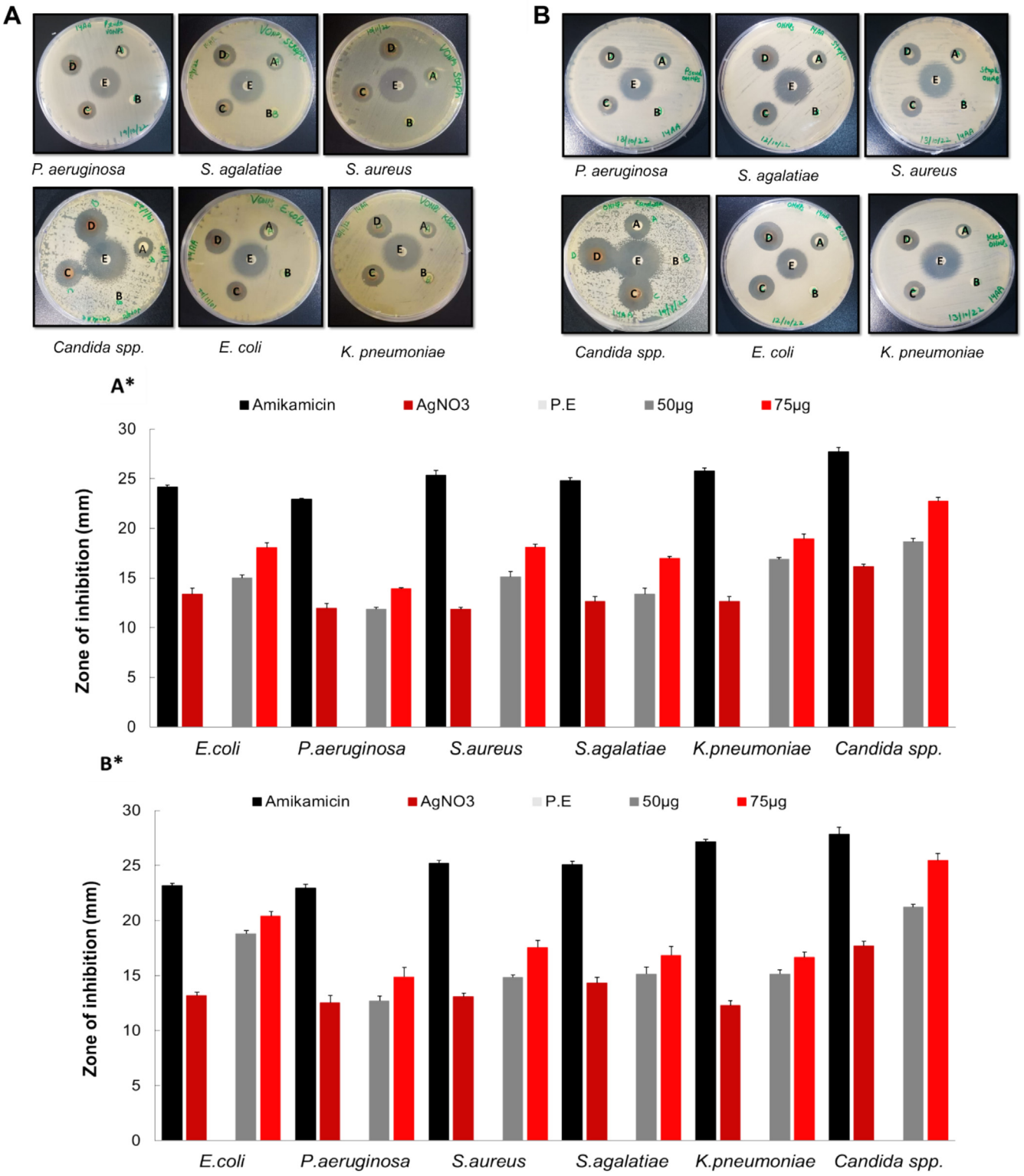

Fig. 4. Antibacterial and antifungal activity of VoL-AgNPs (**A**) and OhRb-AgNPs (**B**). In Fig. **A,** the labeling on the plates depicts that **A** contains 10 mM $AgNO_3$, **B** contains VoL extract, **C** contains 50 µg VoL-AgNPs, **D** contains 75 µg VoL-AgNPs, and **E** contains the antibiotic Amikamicin. In fig. **B**, **A** contains 10 mM $AgNO_3$, **B** contains OhRb extract, **C** contains 50 µg OhRb-AgNPs, **D** contains 75 µg OhRb-AgNPs, and **E** contains the antibiotic Amikamicin, while **A*** and **B*** illustrated a clear ZOI (m m) of VoL-AgNPs and OhRb-AgNPs, respectively, against MDR pathogens *(E. coli, S. aureus, S. agalatiae, K. pneumoniae*, *P. aeruginosa, and Candida* spp.). All tests were carried out in triplicate. Bar plots show the mean values, while the standard deviation is shown as the error bars on bar plots.

Table 1
MIC and MBC of VoL-AgNPs and OhRb-AgNPs.

Tested strains	VoL-AgNPs		OhRb-AgNPs	
	MIC (μg/mL)	MBC (μg/mL)	MIC (μg/mL)	MBC (μg/mL)
E. coli	0.39	0.78	1.56	3.12
P. aeruginosa	0.78	1.56	3.12	6.12
S. aureus	1.56	3.12	3.12	6.12
S. agalatiae	1.56	3.12	1.56	3.12
K. pneumoniae	0.78	1.56	1.56	3.12
Candida spp.	0.78	1.56	3.12	3.12

kacin antibiotics was assessed. The results demonstrated clear zones of inhibition ranging from 12 mm ± 0.636 to 25 mm ± 0.2 82 against various bacterial strains, including *S. aureus*, *E. coli*, and *P. aeruginosa* (Fig. 4A, Fig. 4B).

All the tested bacterial species exhibited a dose-dependent response, where increasing concentrations of AgNPs led to larger zones of inhibition (Fig. 4A*, Fig. 4B*). Table 1 presents the MIC and MBC values for the pathogenic strains.

3.5. Assessing antioxidant and hemolytic potential of synthesized nanoparticles

The antioxidant activity of the synthesized nanoparticles was evaluated using the DPPH assay. The scavenging activities of VoL-AgNPs and OhRb-AgNPs were lowest at concentrations of 75 μg/mL (57 ± 3.98% and 62 ± 1.51%). At the highest concentration of 125 μg/mL, the scavenging activity increased to 83 ± 2.92% for VoL-AgNPs and 79 ± 3.91% for OhRb-AgNPs. Ascorbic acid, used as a reference standard, showed 91.262 ± 0.267% inhibition. The findings demonstrate that the antioxidant activity of both VoL-AgNPs and OhRb-AgNPs significantly increased with higher concentrations (Fig. 5A*, Fig. 5B*).

Triton X-100 and PBS, used as positive and negative controls for hemolysis assay, showed 100% and 0% hemolysis, respectively. When RBCs were exposed to lower concentrations of VoL-AgNPs and OhRb-AgNPs for 60 min, no discernible hemolysis was observed (Fig. 5C, Fig. 5D). The maximum hemolysis (5–7%) was observed only after use of NPs at higher concentration i.e., 300 μg/mL and above, suggesting the degree of hemolysis was dose-dependent.

4. Discussion

The rise of antibiotic resistance in microbes and the adverse effects of synthetic drugs have raised global concerns, especially regarding the treatment of MDR pathogens [2,3]. In the present study, we describe a rapid, cost-effective method for the biogenic synthesis of AgNPs using aqueous extracts of *V. odorata* leaves and *O. hispidum* roots and demonstrate their potential use against MDR pathogens.

The green approach involved a one-step process that effectively synthesized VoL-AgNPs and OhRb-AgNPs within the shortest time of 5–20 min, at 55°C and 60°C respectively, using 10 mM $AgNO_3$. The use of 1–5 mM $AgNO_3$ also led to the synthesis of AgNPs but the time required was higher. This process involved the activation of liberated electrons, resulting in a color change in the solution containing VoL and OhRb extracts. The strong SPR bands observed at 420 nm for VoL-AgNPs and 430 nm for OhRb-AgNPs confirmed the successful synthesis of AgNPs (Fig. 1), consistent with earlier reports [26,27,28]. Here, the pH of the plant extract also played a crucial role in the synthesis process; the highest production of AgNPs occurred at pH 10, which may be attributed to the presence of more free electrons facilitating the reduction processes. This observation aligns well with previous studies [26,27] that reported a similar trend in the UV–Vis spectrum with increasing pH of the plant extracts.

The plant extracts contain bioactive components like proteins, polysaccharides, peptides, phenols, enzymes, and vitamins, which act as both reducing and stabilizing agents, enabling an environmentally friendly synthesis without the need for hazardous chemicals [5,31]. FTIR analysis of the VoL and OhRb extracts, along with their corresponding AgNPs, revealed characteristic peaks attributed to alcohols, phenols, amides, and other functional groups [26,32,33,34,35]. The strong affinity of proteins' carbonyl groups and alcohols' hydroxyl groups for metals suggested the development of a coating surrounding the metal NPs, capping the NPs, and inhibiting their aggregation.

XRD analysis confirmed the crystalline structure of both VoL-AgNPs and OhRb-AgNPs, as indicated by the prominent peaks at specific two-theta values (Fig. 3A, Fig. 3B). Additional peaks were also observed that corresponded to organic compounds in the extracts, responsible for reducing silver ions and forming the AgNPs. The surface charge and stability of VoL-AgNPs and OhRb-AgNPs, when measured using ZP, were found –27.9 mV and –23.5 mV, with polydispersity index (PDI) of 0.25 and 0.246, and average size around 79.92 ± 45.61 and 106 ± 68.01, respectively. AgNPs with a PDI less than 0.3 are regarded as monodisperse, as reported by previous studies [36,37]. The high negative charge on the AgNPs, likely due to the adsorption of free ionic species, provided electrostatic stabilization, preventing particle aggregation [16,18].

The synthesized VoL-AgNPs and OhRb-AgNPs have shown significant antimicrobial activity compared to the corresponding plant extract The MBC ranged between 0.39 and 6.125 μg/mL, while the MIC was 0.781 to 3.125 μg/mL across six pathogenic strains, which was lower than those reported in previous studies, as detailed in **Table S1**. Of note, both AgNPs exhibited a slightly stronger impact against *E. coli* pathogens compared to *S. aureus*. This finding aligns with previous studies reporting that gram-negative bacteria are generally more susceptible to AgNPs than the gram-positive bacteria owing to the presence of a thick layer of peptidoglycan, which acts as a barrier to Ag+ permeation through the cytoplasmic membrane [38,39]. While the exact antibacterial mechanism of AgNPs remains elusive, a compelling explanation lies in the interaction of released Ag^+ ions with essential biomolecules, including sulfur, oxygen, and nitrogen, within microorganisms (Fig. 6). This interaction can lead to structural damage and disruption of essential cellular functions [40,41]. Additionally, AgNPs may exert bactericidal effects through the generation of free radicals that adhere to the bacterial cell wall, creating pits that increase its permeability [42,43]. The ROS generated by Ag^+ ions, acting on the thiol groups of respiratory enzymes, potentially inhibiting their functions [44]. Moreover, exposure to Ag^+ ion induces shrinkage and separation of the cytoplasmic membrane from the cell wall, leading to the release of cellular contents and ultimately causing the disintegration of cell wall [41,42].

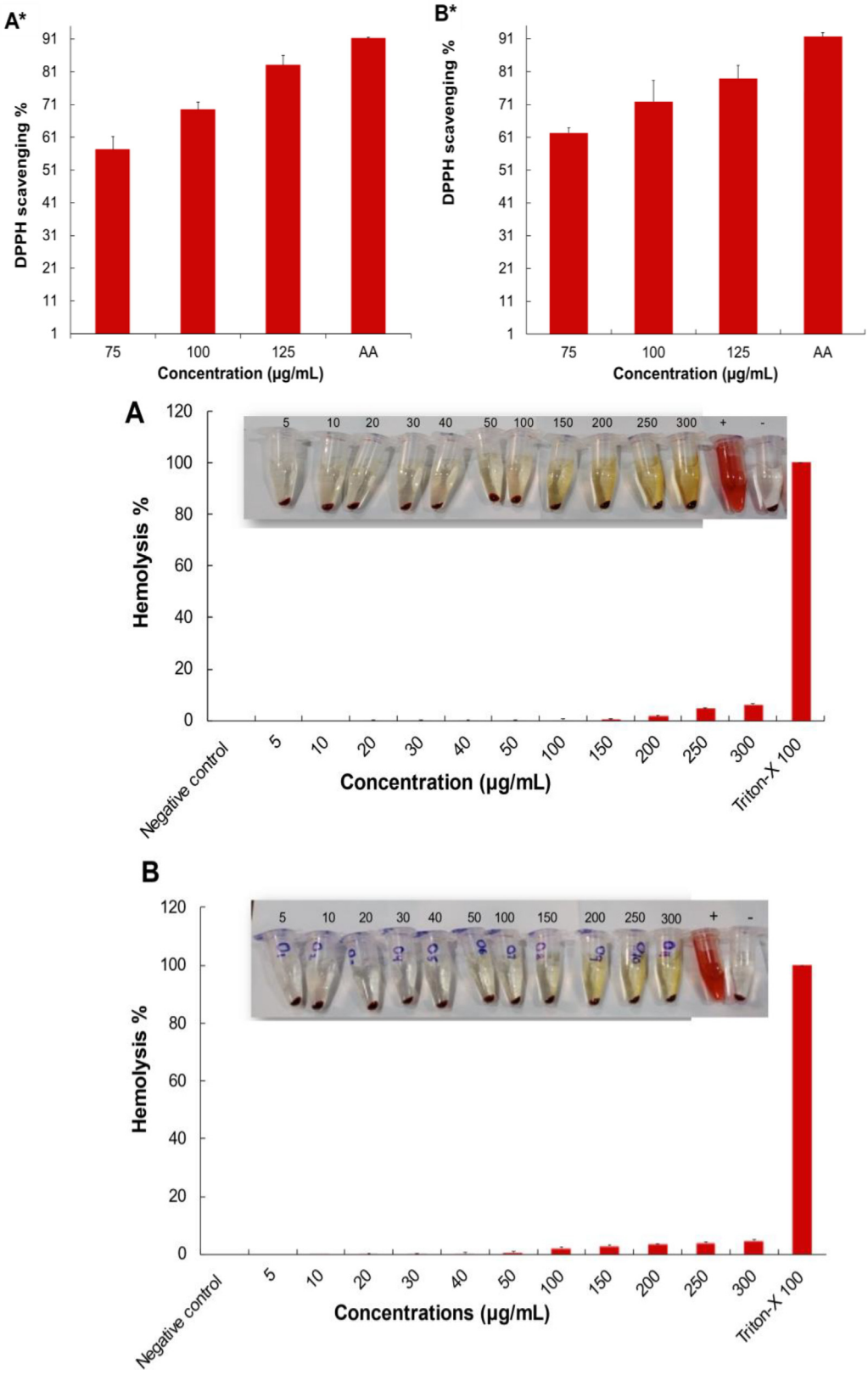

Fig. 5. Antioxidant and hemolytic activity of VoL-AgNPs and OhRb-AgNPs. **A*** and **B*** depicted the antioxidant activity of VoL-AgNPs and OhRb-AgNPs, respectively. While **A** and **B** depicted the hemolytic activity of VoL-AgNPs and OhRb-AgNPs, (A) photos of RBCs after being exposed to different doses of VoL-AgNPs, and (**B**) photos of RBCs after being exposed to different doses of OhRb-AgNPs, together with Triton X-100 and PBS as positive and negative controls. All tests were carried out in triplicate.

Based on qualitative analysis, studies have reported that VoL and OhRb contain an appreciable number of phenols, flavonols, and flavonoids that may contribute to the antioxidant capabilities of VoL-AgNPs and OhRb-AgNPs [22,24,25]. Recently, Dhiman et al. [45] identified the primary phytocomponents of *V. odorata* as anthocyanins, flavonoids, melatonin, coumarins, salicylic acid,

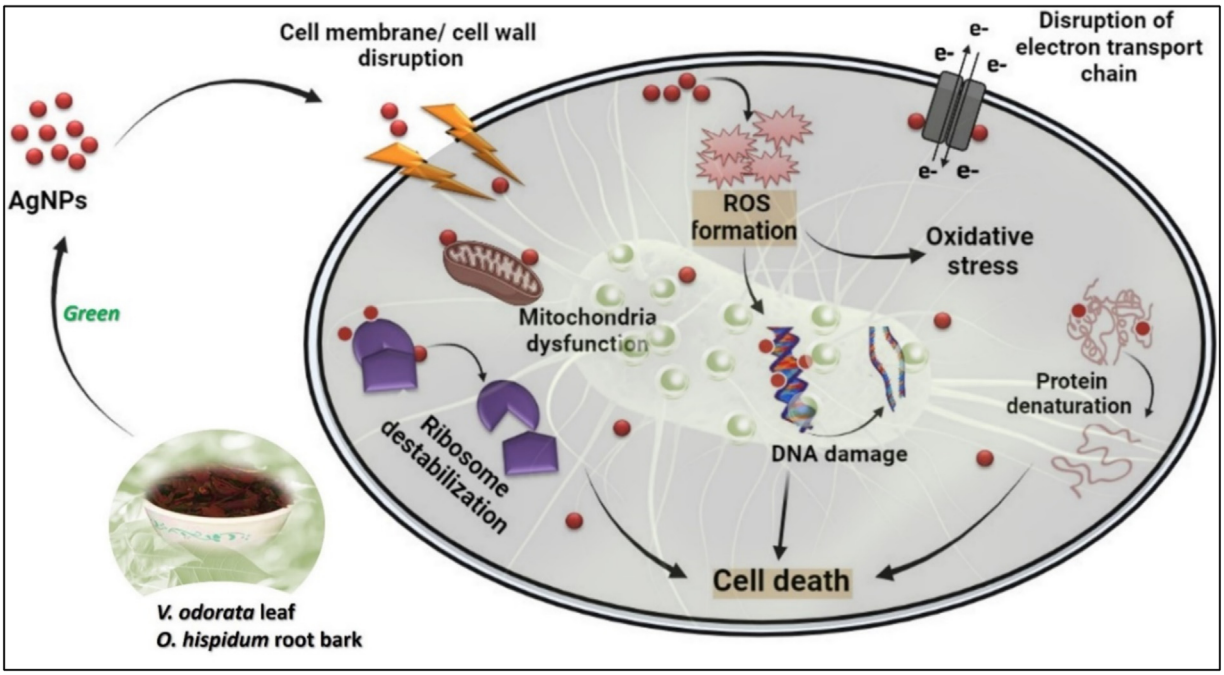

Fig. 6. Possible mechanism of actions underlying the antibacterial effects of synthesized AgNPs.

and alkaloids — compounds that are known to elevate antioxidant levels, reduce harmful oxidants, and suppress pro-inflammatory cytokines (e. g. IL-1β, IL-6, TNF-α). These components, by lowering the nitrite production and activating various neuroprotective mechanisms in the nervous system, offered protection against toxic affronts [45].

Studies have also shown that the strong antioxidant properties of biogenically synthesized NPs enhance their therapeutic effects by reducing oxidative stress in microbial cells [46,47]. The ROS scavenging ability is crucial for the inhibition of oxidative damage, thereby promoting cell survival in healthy tissues while contributing to the antimicrobial action against pathogens. This dual action positions the NPs as effective agents in addressing the infections and reducing inflammation simultaneously [47].

The results of our research align well with previous studies [8], demonstrating that plant-mediated conversion of $AgNO_3$ to nanoscale Ag^+ imparts antioxidant properties to AgNPs. An observed increase in DPPH scavenging activity with higher AgNP concentrations underscores the role of plant extracts in neutralizing free radicals and protecting cells from oxidative damage [47]. The biocompatibility of biosynthesized VoL-AgNPs and OhRb-AgNPs, enhanced by biomolecules acting as natural stabilizers, further supports their potential for biomedical applications [13,23,24] (Fig. 5).

In conclusion, this study contributes to the field of green nanobiotechnology by explaining the successful synthesis of AgNPs using natural plant extracts of VoL and OhRb. The characterized AgNPs demonstrated potent antibacterial and antifungal activity against MDR pathogens, strong antioxidant properties, and low hemolytic activity. These findings suggest their potential use in antimicrobial wound dressings, topical antibiotic formulations, and therapies targeting oxidative stress-related disorders. The environmentally benign green synthesis of AgNPs offers rapid, cost-effective, and biocompatible production suitable for commercial scaling. Further exploration is warranted to fully realize their applications in the pharmaceutical industry.

CRediT authorship contribution statement

Aneeta Andleeb: Writing – original draft, Investigation, Formal analysis. **Aneeza Khalid:** Investigation, Data curation. **Sadia Khalil:** Validation, Investigation. **Hammad Arshad:** Visualization, Validation. **Saima Sadaf:** Writing – review & editing, Supervision, Project administration, Conceptualization.

Financial support

This research was partially supported by a grant (No. 16185/2023) from PakPat World Intellectual Property Protection Services Pakistan.

Declaration of competing interests

Authors have no potential competing interests to declare.

Supplementary material

https://doi.org/10.1016/j.ejbt.2024.12.003.

Data availability

All relevant data or information has been shared in the manuscript.

References

[1] Ajulo S, Awosile B. Global antimicrobial resistance and use surveillance system (GLASS 2022): Investigating the relationship between antimicrobial resistance and antimicrobial consumption data across the participating countries. PLoS One 2024;19(2):. https://doi.org/10.1371/journal.pone.0297921. PMid: 38315668e0297921.

[2] Oliveira M, Antunes W, Mota S, et al. An overview of the recent advances in antimicrobial resistance. Microorganisms 2024;12(9):1920. https://doi.org/10.3390/microorganisms12091920. PMid: 39338594.

[3] Serwecińska L. Antimicrobials and antibiotic-resistant bacteria: A risk to the environment and to public health. Water 2020;12(12):3313. https://doi.org/10.3390/w12123313.

[4] Bayda S, Adeel M, Tuccinardi T, et al. The history of nanoscience and nanotechnology: From chemical-physical applications to nanomedicine. Molecules 2019;25(1):112. https://doi.org/10.3390/molecules25010112. PMid: 31892180.
[5] Natan M, Banin E. From nano to micro: Using nanotechnology to combat microorganisms and their multidrug resistance. FEMS Microbiol Rev 2017;41 (3):302–22. https://doi.org/10.1093/femsre/fux003. PMid: 28419240.
[6] Aguilar-Garay R, Lara-Ortiz LF, Campos-López M, et al. A comprehensive review of silver and gold nanoparticles as effective antibacterial agents. Pharmaceuticals 2024;17(9):1134. https://doi.org/10.3390/ph17091134. PMid: 39338299.
[7] Arshad H, Saleem M, Pasha U, et al. Synthesis of *Aloe vera*-conjugated silver nanoparticles for use against multidrug-resistant microorganisms. Electron J Biotechnol 2022;55:55–64. https://doi.org/10.1016/j.ejbt.2021.11.003.
[8] Altammar KA. A review on nanoparticles: Characteristics, synthesis, applications, and challenges. Front Microbiol 2023;14:. https://doi.org/10.3389/fmicb.2023.1155622. PMid: 371802571155622.
[9] Naysmith A, Mian NS, Rana S. Development of conductive textile fabric using Plackett–Burman optimized green synthesized silver nanoparticles and *in situ* polymerized polypyrrole. Green Chem Lett Rev 2023;16(1):. https://doi.org/10.1080/17518253.2022.2158690 2158690.
[10] Laib I, Ali BD, Boudebia O. Green synthesis of silver nanoparticles using *Helianthemum lippii* extracts (Hl-NPs): Characterization, antioxidant and antibacterial activities, and study of interaction with DNA. J Organomet Chem 2023;986:. https://doi.org/10.1016/j.jorganchem.2023.122619 122619.
[11] Samreen AI, Khan SA, et al. Green synthesized silver nanoparticles from *Phoenix dactylifera* synergistically interact with bioactive extract of *Punica granatum* against bacterial virulence and biofilm development. Microb Pathog 2024;192:. https://doi.org/10.1016/j.micpath.2024.106708. PMid: 38782213106708.
[12] Abbas M, Hussain T, Iqbal J, et al. Synthesis of silver nanoparticle from *Allium sativum* as an eco-benign agent for biological applications. Pol J Environ Stud 2022;31(1):533–8. https://doi.org/10.15244/pjoes/135764.
[13] Zhao H, Su H, Ahmeda A, et al. Biosynthesis of copper nanoparticles using *Allium eriophyllum* Boiss leaf aqueous extract: Characterization and analysis of their antimicrobial and cutaneous wound-healing potentials. Appl Organomet Chem 2022;36(12):e5587.
[14] Tavanappanavar AN, Mulla SI, Seth SC, et al. Phytochemical analysis, GC-MS profile and determination of antibacterial, antifungal, anti-inflammatory, antioxidant activities of peel and seeds extracts (chloroform and ethyl acetate) of *Tamarindus indica* L. Saudi J Biol Sci 2024;31(1):. https://doi.org/10.1016/j.sjbs.2023.103878. PMid: 38125735103878.
[15] Dehnoee A, Kalbasi JR, Zangeneh MM, et al. Characterization, anti-lung cancer activity, and cytotoxicity of bio-synthesized copper nanoparticles by *Thymus fedtschenkoi* leaf extract. J Clust Sci 2024;35:863–74. https://doi.org/10.1007/s10876-023-02512-w.
[16] Wang G, Ahmeda A, Malek Z, et al. Chemical characterization and therapeutic properties of *Achillea biebersteinii* leaf aqueous extract synthesized copper nanoparticles against methamphetamine-induced cell death in PC12: A study in the nanotechnology and neurology fields. Appl Organomet Chem 2020;34 (4):e5488. https://doi.org/10.1002/aoc.5488.
[17] Alshameri AW, Owais M, Altaf I, et al. *Rumex nervosus* mediated green synthesis of silver nanoparticles and evaluation of its in vitro antibacterial, and cytotoxic activity. OpenNano 2022;8:. https://doi.org/10.1016/j.onano.2022.100084 100084.
[18] Khane Y, Benouis K, Albukhaty S, et al. Green synthesis of silver nanoparticles using aqueous *Citrus limon* zest extract: Characterization and evaluation of their antioxidant and antimicrobial properties. Nanomaterials 2022;12 (12):2013. https://doi.org/10.3390/nano12122013. PMid: 35745352.
[19] Jalab J, Abdelwahed W, Kitaz A, et al. Green synthesis of silver nanoparticles using aqueous extract of *Acacia cyanophylla* and its antibacterial activity. Heliyon 2021;7(9):. https://doi.org/10.1016/j.heliyon.2021.e08033. PMid: 34611564e08033.
[20] Hashemi Z, Mohammadyan M, Naderi S, et al. Green synthesis of silver nanoparticles using *Ferula persica* extract (Fp-NPs): Characterization, antibacterial, antileishmanial, and *in vitro* anticancer activities. Mater Today Commun 2021;27:. https://doi.org/10.1016/j.mtcomm.2021.102264 102264.
[21] Dehnoee A, Kalbasi RJ, Zangeneh MM, et al. One-step synthesis of silver nanostructures using *Heracleum persicum* fruit extract, their cytotoxic activity, anti-cancer and anti-oxidant activities. Micro Nano Lett 2023;18(1):. https://doi.org/10.1049/mna2.12153 e12153.
[22] Salwan R, Rana A, Saini R, et al. Diversity analysis of endophytes with antimicrobial and antioxidant potential from *Viola odorata*: An endemic plant species of the Himalayas. Braz J Microbiol 2023;54(3):2361–74. https://doi.org/10.1007/s42770-023-01010-5. PMid: 37227628.
[23] Zahra T, Ahmad KS, Sharif S. Identification and implication of organic compounds of *Viola odorata*: A potential source for bio-fabrication of nickel oxide nanoparticles. Appl Nanosci 2021;11:1593–603. https://doi.org/10.1007/s13204-021-01777-9.
[24] Kumar N, Kumar R, Kishore K. *Onosma* L.: A review of phytochemistry and ethnopharmacology. Pharmacogn Rev 2013;7(14):140–51. https://doi.org/10.4103/0973-7847.120513. PMid: 24347922.
[25] Wazir NU, Khan AI, Javed A, et al. *Onosma hispidum* L. extract reverses hyperlipidemia, hypertension, and associated vascular dysfunction in rats. Saudi J Biol Sci 2023;30(8):. https://doi.org/10.1016/j.sjbs.2023.103712. PMid: 37405138103712.
[26] Arshad H, Sami MA, Sadaf S, et al. *Salvadora persica* mediated synthesis of silver nanoparticles and their antimicrobial efficacy. Sci Rep 2021;11:5996. https://doi.org/10.1038/s41598-021-85584-w.
[27] Arshad H, Sadaf S, Hassan U. De-novo fabrication of sunlight irradiated silver nanoparticles and their efficacy against *E. coli* and *S. epidermidis*. Sci Rep 2022;12:676. https://doi.org/10.1038/s41598-021-04674-x. PMid: 35027620.
[28] Khare S, Singh RK, Prakash O. Green synthesis, characterization and biocompatibility evaluation of silver nanoparticles using radish seeds. Results Chem 2022;4:. https://doi.org/10.1016/j.rechem.2022.100447 100447.
[29] Sreelekha E, George B, Shyam A, et al. A comparative study on the synthesis, characterization, and antioxidant activity of green and chemically synthesized silver nanoparticles. BioNanoSci 2021;11:489–96. https://doi.org/10.1007/s12668-021-00824-7.
[30] Parthiban E, Manivannan N, Ramanibai R, et al. Green synthesis of silver-nanoparticles from *Annona reticulata* leaves aqueous extract and its mosquito larvicidal and anti-microbial activity on human pathogens. Biotechnol Rep 2018;21:. https://doi.org/10.1016/j.btre.2018.e00297. PMid: 30581768e00297.
[31] Karnjana K, Jewboonchu J, Niyomtham N, et al. The potency of herbal extracts and its green synthesized nanoparticle formulation as antibacterial agents against *Streptococcus mutans* associated biofilms. Biotechnol Rep 2023;37:. https://doi.org/10.1016/j.btre.2022.e00777. PMid: 36582762e00777.
[32] Arshad H, Sadaf S, Hassan U. Synthesis and immobilization of silver nanoparticles on filter paper and surgical masks for antimicrobial applications. In: IEEE 17th International Conference on Nano/Micro Engineered and Molecular Systems (NEMS); 2022 April 14–17; Taoyuan, Taiwan: IEEE; 2022. p. 301–305. https://doi.org/10.1109/NEMS54180.2022.9791147.
[33] Gajendran B, Durai P, Varier KM, et al. Green synthesis of silver nanoparticle from *Datura inoxia* flower extract and its cytotoxic activity. BioNanoScience 2019;9:564–72. https://doi.org/10.1007/s12668-019-00645-9.
[34] George IE, Cherian T, Ragavendran C, et al. One-pot green synthesis of silver nanoparticles using brittle star *Ophiocoma scolopendrina*: Assessing biological potentialities of antibacterial, antioxidant, anti-diabetic and catalytic degradation of organic dyes. Heliyon 2023;9(3):. https://doi.org/10.1016/j.heliyon.2023.e14538. PMid: 36967974e14538.
[35] Clarance P, Luvankar B, Sales J, et al. Green synthesis and characterization of gold nanoparticles using endophytic fungi *Fusarium solani* and its *in-vitro* anticancer and biomedical applications. Saudi J Biol Sci 2020;27(2):706–12. https://doi.org/10.1016/j.sjbs.2019.12.026.
[36] Manosalva N, Tortella G, Diez MC, et al. Green synthesis of silver nanoparticles: Effect of synthesis reaction parameters on antimicrobial activity. World J Microbiol Biotechnol 2019;35(6):88. https://doi.org/10.1007/s11274-019-2664-3. PMid: 31134435.
[37] Vera-Nuñez LDC, Cornejo-Ruiz JO, Arenas-Chávez CA, et al. Green synthesis of a novel silver nanoparticle conjugated with *Thelypteris glandulosolanosa* (Raqui-Raqui): Preliminary characterization and anticancer activity. Processes 2022;10(7):1308. https://doi.org/10.3390/pr10071308.
[38] Audtarat S, Hongsachart P, Dasri T, et al. Green synthesis of silver nanoparticles loaded into bacterial cellulose for antimicrobial application. Nanocomposites 2022;8(1):34–46. https://doi.org/10.1080/20550324.2022.2055375.
[39] Erjaee H, Rajaian H, Nazifi S. Synthesis and characterization of novel silver nanoparticles using *Chamaemelum nobile* extract for antibacterial application. Adv Nat Sci Nanosci Nanotechnol 2017;8(2):. https://doi.org/10.1088/2043-6254/aa690b 025004.
[40] Agarwal H, Menon S, Kumar SV, et al. Mechanistic study on antibacterial action of zinc oxide nanoparticles synthesized using green route. Chem Biol Interact 2018;286:60–70. https://doi.org/10.1016/j.cbi.2018.03.008. PMid: 29551637.
[41] Hassanvand A, Saadatmand S, Yazdi HL, et al. Investigation of antioxidant, antimicrobial and anticancer potential of silver nanoparticles synthesized by *Viola tricolor* L. extract. J Agric Sci Technol 2022;24(4):885–900.
[42] Santhosh A, Sandeep S, Manukumar H, et al. Green synthesis of silver nanoparticles using cow urine: Antimicrobial and blood biocompatibility studies. JCIS Open 2021;3:. https://doi.org/10.1016/j.jciso.2021.100023 100023.
[43] Rashid MI, Mujawar LH, Rehan ZA, et al. One-step synthesis of silver nanoparticles using *Phoenix dactylifera* leaves extract and their enhanced bactericidal activity. J Mol Liq 2016;223:1114–22. https://doi.org/10.1016/j.molliq.2016.09.030.
[44] Andleeb A, Andleeb A, Asghar S, et al. A systematic review of biosynthesized metallic nanoparticles as a promising anti-cancer-strategy. Cancers 2021;13 (11):2818. https://doi.org/10.3390/cancers13112818. PMid: 34198769.
[45] Dhiman S, Singla S, Kumar I, et al. Protection of *Viola odorata* L. against neurodegenerative diseases: Potential of the extract and major phytoconstituents. Clin Complement Med Pharmacol 2023;3(3):. https://doi.org/10.1016/j.ccmp.2023.100105 100105.
[46] Rezaei F, Tajik H, Shahbazi Y. Intelligent double-layer polymers based on carboxymethyl cellulose-cellulose nanocrystals film and poly(lactic acid)-*Viola odorata* petal anthocyanins nanofibers to monitor food freshness. Int J Biol Macromol 2023;252:. https://doi.org/10.1016/j.ijbiomac.2023.126512. PMid: 37633548126512.
[47] Tiwana G, Cock IE, Cheesman MJ. *Phyllanthus niruri* Linn.: Antibacterial activity, phytochemistry, and enhanced antibiotic combinatorial strategies. Antibiotics 2024;13(7):654. https://doi.org/10.3390/antibiotics13070654. PMid: 39061336.